Chapter

Variation of Sensitivity of a MEMS Capacitive Accelerometer Based Microphone with Suspension System Topology

Apoorva Dwivedi, Prateek Asthana, Gargi Khanna and Tarun Chaudhary

Abstract

The present research seeks to improve a highly sensitive MEMS capacitive accelerometer as a probable completely implantable hearing aid microphone. The research analyses the effect of different suspension system topologies on accelerometer efficiency. The topology of folded beam suspension is considered to be the most suitable for the proposed system. The design factors such as weight, height and resonant frequency are considered to make the accelerometer an effective biomedical system which can be completely implanted with COMSOL MULTIPHYSICS 4.2 the optimized system is simulated and validated. The accelerometer occupies 1mm^2 of sensing area and achieves a nominal capacitance of 5.30 pF and an optimized capacitive sensitivity of 6.89fF.

Keywords: Microelectromechanical system (MEMS), totally implantable hearing aid (TIHA), capacitive accelerometer, mechanical amplification, microlever, sound pressure level (SPL)

1. Introduction

The universe is perceived by means of the five senses. By conjunction these five senses determine the nature of our world experience. If some meaning is lacking it removes a whole aspect of life. Similarly, the quality of life experience for people with hearing loss is significantly diminished. An individual with a completely functioning sense of hearing can hardly understand the suffering of those living with the hearing impairment. WHO reports that 15 percent of the world's adults, or approximately 766 million people, are experiencing the substantial loss of audience [1]. In India this figure is alarmingly more than 63 million, according to Varshney [2]. In most cases of hearing loss, traditional hearing aids may offer effective rehabilitation, but the societal stigma linked with wearing external hearing aids prohibits several patients from even talking about such devices. Consequently, semi-implantable middle ear and cochlear prosthetic devices are increasingly approved. Over the years, curiosity in middle ear implants has grown significantly to facilitate patients with traditional hearing aids who do not get sufficient assistance [3].

Electromagnetics-based middle ear implants [4, 5] and Piezoelectric [6, 7] have been developed for hearing loss gain. Such techniques, however, do not offer protection from damage to cochlear hair cells in hearing loss. While current cochlear implants that are partially implantable treat injured hair cells in the cochlea through direct stimulation of the auditory nerve, they remain dependent on external microphone, speech processor, and radiofrequency (RF) coils [8]. The ever-present need for invisibility has fuelled the creation of a completely implantable hearing aid to free the patient from the extreme loss of hearing without any social stigma.

Although current partially implantable cochlear implants are being increaasingly used, their usage of an external microphone, speech processor and radio frequency (RF) coils has still not addressed the issue of social stigma and embarrassment. The need to provide the users freedom from the psychological discomfort, physical inconvenience and offer improved performance has accelerated the exploration and growth of fully implantable hearing aids (FIHAs). The FIHAs, with all the elements implanted internally and using the natural sound conduction of the body, eliminate many of the issues like sound filtering, improved sound amplification, problem of feedback, ringing issues and social prejudice faced in conventional hearing aids.

The MEMS capacitive accelerometer described in the paper is designed to be placed on umbo to act as a middle ear microphone as shown in **Figure 1**. Optimizing the geometry of the device has already increased the performance of the accelerometer [9–12]. This article studies the effect of various suspension system (spring) topologies on the sensitivity of the accelerometer and then proposes the most suitable suspension system for enhanced performance. The optimized model satisfies the requisite design requirements regarding the fully implantable microphone's surgical placement.

The article consists of 5 parts. The first segment discusses the implementation of hearing aids based on MEMS which are entirely implantable. The second segment describes the development of hearing aids which are entirely implantable. The third

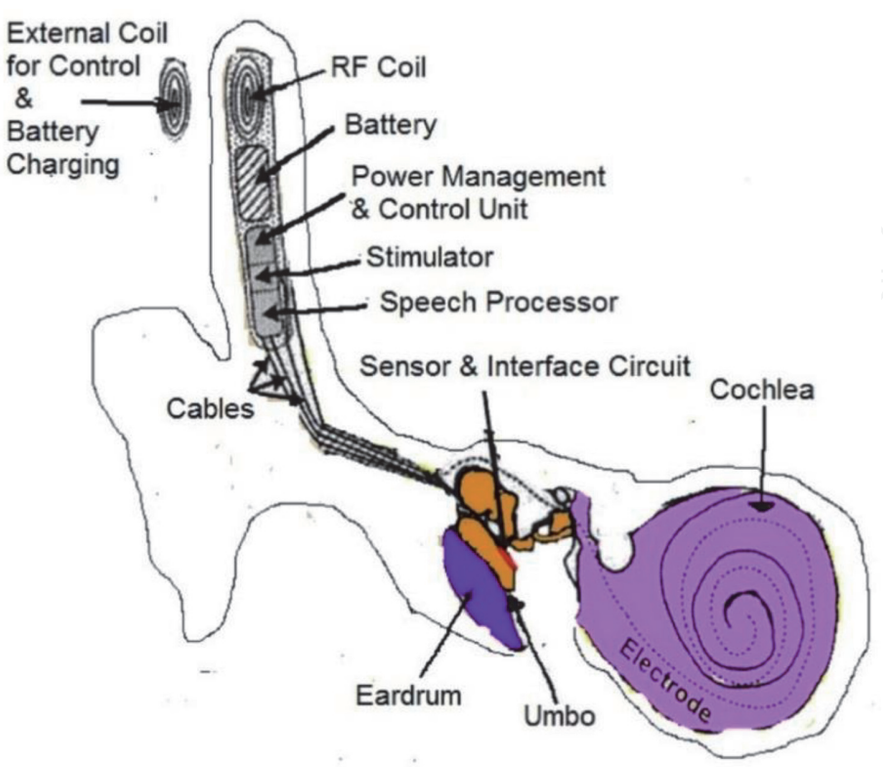

Figure 1.
Proposed fully implantable microphone in middle ear.

section addresses the sensor's operating theory and assessing the stiffness constant as a suspension mechanism for various springs. The fourth section explains the outcomes of the modelling and simulation followed by a conclusion in Section 5.

2. Development of totally implantable hearing aids

Various forms of TIHAs have been documented in the literature, such as Totally Implantable Communication Assistance (TICA) [13], Totally Implantable Cochlear Implant (TICI/TIKI) [14], Carina [15, 16], and Esteem [15–17]. Carina and TIKI, implanted in the temporal bone under the skin, experience severe body noise amplification during mastication, sound attenuation and head contact distortion due to the skin's sound-filtering effect. TICA and Esteem, when implanted in the ear canal or ossicular chain, solved those issues. Yet they are susceptible to the feedback problem between the embedded microphone and the sound source. The literature recorded MEMS capacitive sensor based microphones [18–20]. They are put straight on the umbo. Regrettably, this approach can induce a significant damping effect on the frequency response of the ossicular middle ear chain at frequencies above 1 kHz due to the loading of sensor weight on the umbo [18–20]. Yip et al. [21] have suggested a piezoelectric sensor as a microphone of the FIHA. The umbo is placed at one end of the microphone, and the middle- wall is connected at the other end. The microphone, however, suffers from the problem of feedback, because it resembles Esteem. Woo et al. [22] introduces a trans- microphone. It consists of a ventilation tube mounted in the eardrum along with a connected acoustic duct with an electret microphone at the end extending into the middle-ear cavity. The method presented potential benefits, such as comparatively quick surgery, exceptional sound collection and protection from any outside impact. The possible disadvantages, however, contain the tube dropping into the ear canal or middle ear cavity, the fluid entering the tube, and the sensitivity loss, and the cerumen covering the microphone, and inhibiting sound collection. Koch et al. [23] presents a piezoelectric transducer which is implanted into the incudostapedial joint gap. While it provides advantages such as relatively easy installation and revocable surgery, the transducer suffers from low frequency (<1 KHz) output degradation.

From the literature review it was observed that the system proposed by Young et al. [20] using the capacitive sensing scheme used provides many advantages over the other types: fairly simple mechanical structure compared to other types; henceforth easy manufacturing, excellent linearity, good noise efficiency, a reduced amount of power consumption and very small temperature-induced drift. Together with the mechanical elements, the capacitance sensing signal conditioning circuit can also be monolithically mounted on the same substratum. The only downside of Young et al.'s proposed model is the mass loading effect.

The present paper proposes changes to Young's approach by using different topologies of the suspension system taking into account their effect on device sensitivity. The impact of loading can be evaded by maintaining the sensor's total packed mass below 20 mg. In addition, the overall prototype microsystem will show a packed dimension of less than 3.5 mm for implantation on the umbo without impacting other structures inside the middle ear cavity. The tip of the umbo usually has a scale between 1.5 mm and 2 mm. The accelerometer is therefore built within a compact 1 mm/1 mm band. Absolute umbo acceleration along the primary axis is around 1 g [18–20]. As per audiologists, the loudness of regular human communication is about 60 dB SPL (sound pressure level), and the typical voice speech is in the frequency range from 500 Hz to 8000 Hz. The accelerometer is worked within the normal range of speech conversation frequency, in which the response is flat.

Consequently, the accelerometer's resonant frequency is chosen to be higher than the standard frequency range for human conversation. Yet the resonant frequency can not be too high; then the displacement of the confirmed mass decreases. The accelerometer was therefore designed to set the resonant frequency at about 10,000 Hz.

3. Working principle of the device

3.1 Structural design

The comb drive capacitive accelerometer used in this work includes four folded beams as a suspension device and a handheld finger seismic mass as shown in **Figure 2**. A comb drive structure consists of a set of pairs of capacitive fingers instead of one capacitive plate. Another set is fixed, and the other set remains movable. Further the two anchors are set also. The four folded beams bind each of the anchors to the movable central seismic mass. Let's say; x1 is the distances between the set finger and the movable finger on the left and x2 on the right.

On the umbo is set the capacitive accelerometer. The eardrum vibrates in response to incoming sound causing the umbo to vibrate along with it. The pressure coming in exerts a force on the sensor. The seismic mass with the moving fingers shifts in the direction of body force under the impact of this force, which changes the power between the moving and the fixed finger. The capacitance shift is calculated using a low noise electronic interface circuitry.

The input umbo acceleration a, causes a body force F_{ext} to act on the accelerometer with effective mass M_e.

$$F_{ext} = M_e a \tag{1}$$

The acceleration applied displaces the seismic mass by a distance of Δx from its mean spot. The force needed to displace the seismic mass is given.

$$F_{spring} = k_e \Delta x \tag{2}$$

where k_e is the effective spring constant. In the equilibrium condition when $F_{ext} = F_{spring}$, we get.

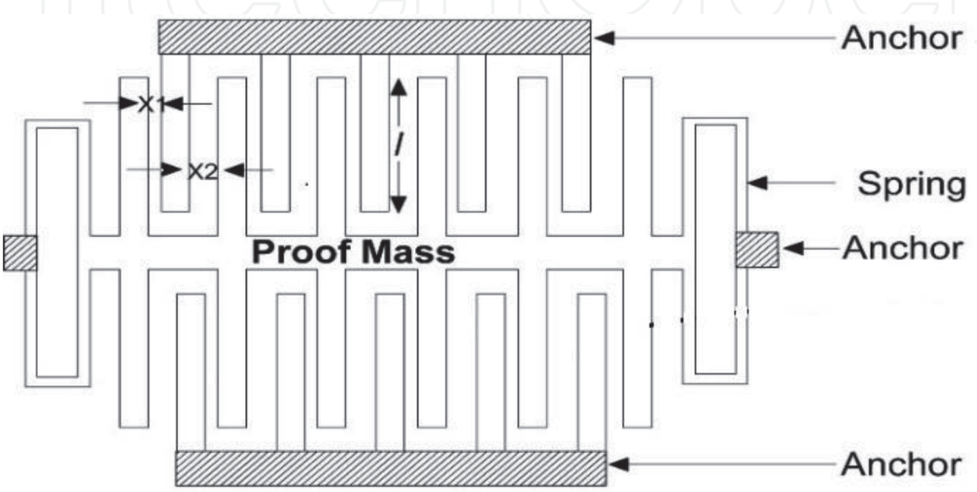

Figure 2.
Prototype of the capacitive accelerometer.

$$\frac{\Delta x}{a} = \frac{M_e}{k_e} \tag{3}$$

That also reflects the sensitivity of the unit to mechanical/displacement. The Eq. (3) shows that the device's displacement sensitivity has a direct relation to the seismic mass and an inverse relationship to the accelerometer's stiffness constant. Hence, the device's displacement sensitivity can be amplified by increasing the seismic mass and reducing the system's stiffness constant. The displacement sensitivity is inversely proportional to the square of the resonant angular frequency.

$$\frac{\Delta x}{a} = \frac{1}{\omega_0^2} = \frac{M_e}{k_e} \tag{4}$$

$$\omega_0 = \sqrt{\frac{k_e}{M_e}} \tag{5}$$

where ω_0 is the resonant angular frequency.

The resonant frequency of the sensor is given as $f_0 = \frac{1}{2\pi}\sqrt{\frac{k_e}{M_e}}$.

The values of mass and stiffness constant are determined to keep the resonant frequency at 10000 Hz.

3.2 Stiffness constant evaluation

The seismic mass can be suspended using various topology suspension systems (springs) based on 1) geometry: standard folded and round folded; 2) beam orientation: standard folded and inverted folded, and 3) series combination of springs. Each of these different types of suspension systems produces a specific accelerometer geometry which affects the sensitivity of the device.

3.2.1 Folded beam

Figure 3 indicates a folded beam-structure. The structure of the folded beam was resolved into three constituents organized in a row.

The accelerometer is composed of four folded beams as springs. The stiffness constant ($k_{1/4}$) of one such folded beam is given in Eq. (6) as.

$$\frac{1}{k_{1/4}} = \frac{1}{k_{c1}} + \frac{1}{k_{c2}} + \frac{1}{k_{c3}} \tag{6}$$

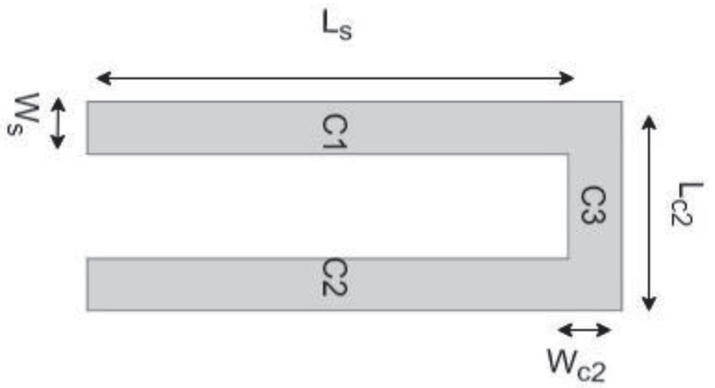

Figure 3.
A folded beam structure.

where k_{c1}, k_{c2}, and k_{c3} are the stiffness constants [23] for the constituent 1 (C1), constituent 2 (C2) and constituent 3 (C3) respectively given as.

$$\frac{1}{k_{c1}} = \frac{{L_s}^3}{12EI_s} + \frac{6(1+\mu)L_s}{5W_s} \tag{7}$$

As C1 and C2 constituents are of same dimensions, the stiffness constant of both these components are equal as given below.

$$\frac{1}{k_{c3}} = \frac{1}{k_{c1}} \tag{8}$$

$$\frac{1}{k_{c2}} = \frac{L_{c2}}{EA_{c2}} - \frac{L_s L_{c2}^2}{4EI_{c2}} \tag{9}$$

where E is the modulus of elasticity of the material, L_s is the length of the spring beam, L_{c2} is the length of the transverse bar, W_{c2} is the width of the bar, W_s is the width of the spring beam, $I = \frac{tW_s{}^3}{12}$ is the moment of inertia of component 1, $I_{c2} = \frac{tW_{c2}{}^3}{12}$ is the moment of inertia of component 2, $A_{c2} = tW_{c2}$ is the area of cross-section of component 2. W_{c2} is the same as W_s.

As the four springs have the same geometry and are made of same material, the effective stiffness constant k_e [24] is evaluated by Eqs. (10) and (11) as.

$$\frac{1}{k_e} = \frac{1}{4k_{1/4}} \tag{10}$$

$$\frac{1}{k_e} = \frac{1}{Et}\left(\frac{{L_s}^3}{2{W_s}^3} + \frac{3(1+\mu)}{5W_s} + \frac{L_{c2}}{4W_{c2}} - \frac{3L_s {L^2}_{c2}}{4W_{c2}^3}\right) \tag{11}$$

3.2.2 Inverted folded beam

The inverted folded beam, as seen in **Figure 4**, differs from folded beam only in terms of suspension orientation. The constant of stiffness is measured the same way as for the regular folded beam. In this case, it will require two supplementary support constituents identical to component 2 to connect the beam to the seismic mass and anchor. Adding both of these constituents gives us the constant stiffness as.

$$\frac{1}{k_e} = \frac{1}{Et}\left(\frac{{L_s}^3}{2{W_s}^3} + \frac{3(1+\mu)}{5W_s} + \frac{3L_{c2}}{4W_{c2}} - \frac{9L_s {L^2}_{c2}}{4W_{c2}^3}\right) \tag{12}$$

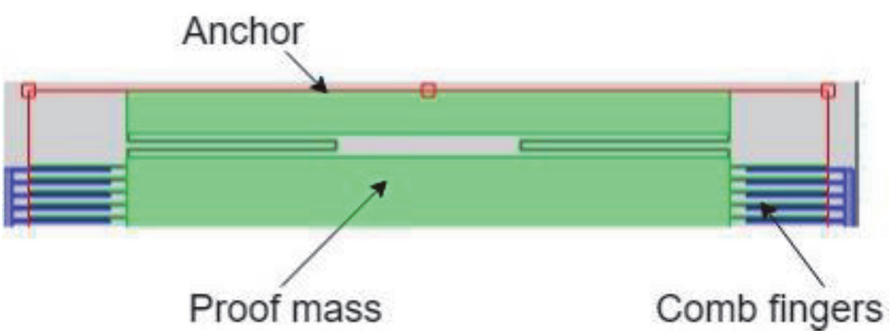

Figure 4.
An inverted folded beam as a suspension system in an accelerometer.

3.2.3 Round folded beam

A circular folded beam is made of round edges rather than rectangular edges as seen in **Figure 5**. For constituent 1 and constituent 3 the stiffness constants are identical to the regular folded beam.

The stiffness constant for the constituent 2 is evaluated by [25] as.

$$\frac{1}{k_{c2}} = \frac{24r^3}{{W_s}^3}\left(\frac{\pi}{16} - \frac{1}{\pi} + \frac{1}{24\pi}\right) + \frac{3\pi L_s^2 r}{4W_s^3} \tag{13}$$

The total stiffness constant is thus obtained by Eq. (14).

$$\frac{1}{k_e} = \frac{1}{Et}\left(\frac{{L_s}^3}{2{W_s}^3} + \frac{3(1+\mu)}{5W_s} + \frac{24r^3}{{W_s}^3}\left(\frac{\pi}{16} - \frac{1}{\pi} + \frac{1}{24\pi}\right) + \frac{3\pi L_s^2 r}{4W_s^3}\right) \tag{14}$$

3.2.4 Series combination of springs

From Eq. (4) it is detected that the displacement of the seismic mass increases with decreasing stiffness. Thus, a sequence of combinations of springs may be used to improve evidence mass displacement. Since the area of the proposed system is limited, however, the addition of a series of combinations of springs leads to a reduction in the width of the seismic mass resulting in a decrease in the seismic mass and thus a decrease in the displacement as shown in **Table 1**. Therefore a compromise is needed when choosing the combination of the pair. Some of the combinations from the sequence are shown in **Figure 6**.

The stiffness constants and seismic mass width for different arrangements of springs are given by **Table 1**. W_{pm} denotes the width of the seismic mass, W_a is the

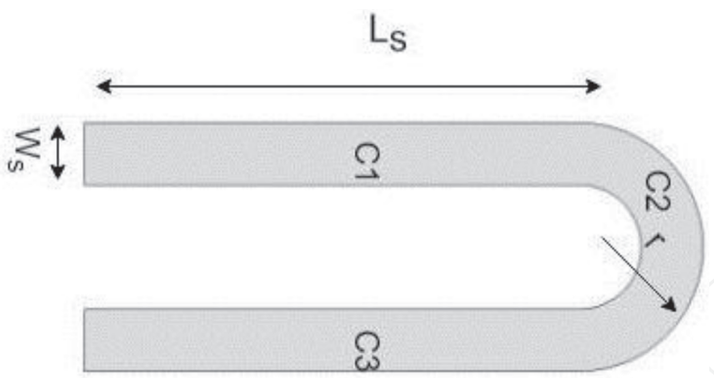

Figure 5.
A round folded beam structure.

Number of springs in series	The width of the proof mass (m)	Stiffness constant
1	$W_{pm} = 1000 \times 10^{-6} - 2(W_a + 2W_s + D_b)$	k_e
2	$W_{pm} = 1000 \times 10^{-6} - 4(W_a + 2W_s + D_b) - 2D_b$	$k_e/2$
3	$W_{pm} = 1000 \times 10^{-6} - 6(W_a + 2W_s + D_b) - 4D_b$	$k_e/3$
4	$W_{pm} = 1000 \times 10^{-6} - 8(W_a + 2W_s + D_b) - 6D_b$	$k_e/4$
5	$W_{pm} = 1000 \times 10^{-6} - 10(W_a + 2W_s + D_b) - 8D_b$	$k_e/5$

Table 1.
Proof mass widths and stiffness constants for a different combination of springs.

(a)

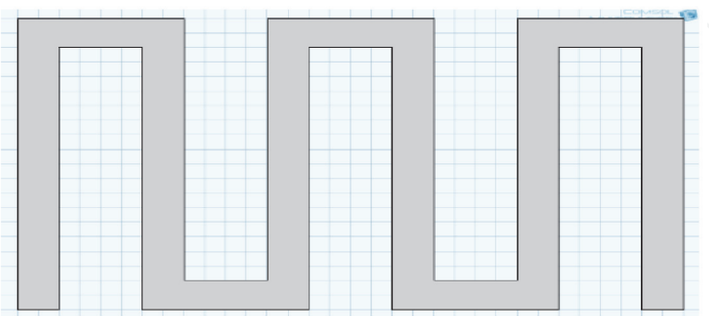

(b)

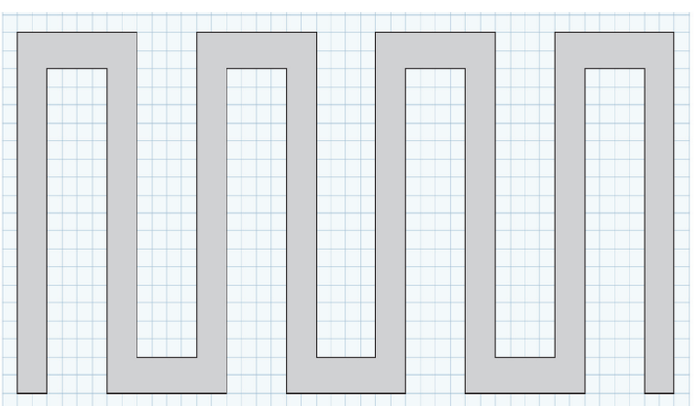

(c)

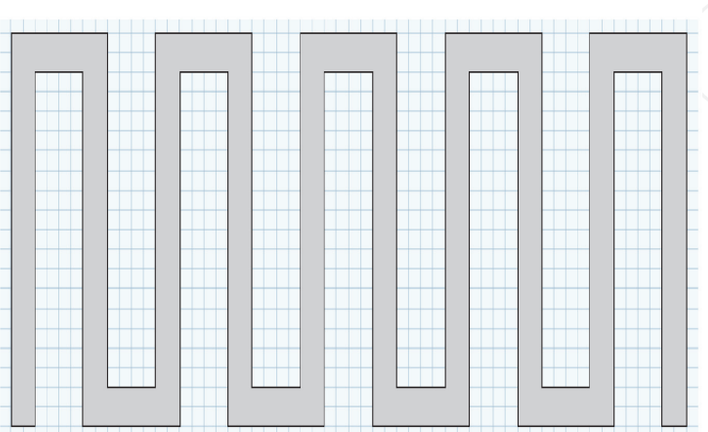

(d)

Figure 6.
Different series combination of springs (a) two springs, (b) three springs, (c) four springs and (d) five springs in series respectively.

width of the anchor, W_s is the width of the spring beam, and D_b is the gap spacing within the spring beam.

The effective mass of the folded suspension beam has been calculated by using the Rayleigh principle [24] as shown in Eqs. (15)-(17).

Effective mass due to the beam is.

$$M_{b,e} = \frac{13\rho W_s t L_s}{35} \tag{15}$$

Effective mass due to the transverse bar is.

$$M_{t,e} = \frac{1}{3}\rho W_{c2} t L_{c2} \tag{16}$$

The accelerometer's effective mass consists mainly of the evidence mass and smaller spring beam contributions. Consider the folded beam segment shown in **Figure 4**. Therefore the total effective accelerometer mass is.

$$M_e = 8M_{b,e} + 4M_{t,e} + M_{pm} \tag{17}$$

Four folded beams exist, with each beam having two lateral parts. Consequently, the whole of eight sections add to the effective mass represented in Eq. (17) by the first term. Each folded beam has a transverse section. So, as seen in the second term in Eq. (17), the mass due to the transverse section is multiplied by four times. The seismic mass contains the mass on either side of the seismic mass due to the rectangular disk, and the mass due to the comb fingers. The test of proof is.

$$M_{pm} = t\rho\left(L_{pm}W_{pm} + 2N_f L_f W_f\right) \tag{18}$$

where L_f is the length of the finger, L_{pm} is the length of the seismic mass, and W_{pm} is the width of the seismic mass. The number of sensing fingers N_f on each side of the seismic mass is restricted by the width of the central seismic mass. Depending on the various constraints, they can be calculated as.

$$N_f = \left(W_{pm} - 2p_f\right)/\left(2W_f + x_1 + x_2\right) \tag{19}$$

The seismic mass for other spring combinations can be determined along similar lines.

3.3 Capacitance evaluation

The sum of the capacitance from each side depends on the finger width W_f, finger overlap length L_{f0}, dielectric constant K, relative permittivity $\epsilon_{0,}$ device layer thickness t, the number of sensing fingers N_f and the air gap between adjacent fingers. It can be expressed by.

$$C_{t0} = \left(C_0 + C_{pm}\right) \tag{20}$$

where C_0 is the capacitance between the fixed and movable fingers as depicted by Eq. (21) and C_{pm} is the capacitance between the movable fingers and the seismic mass body as shown by Eq. (22) in **Figure 7**.

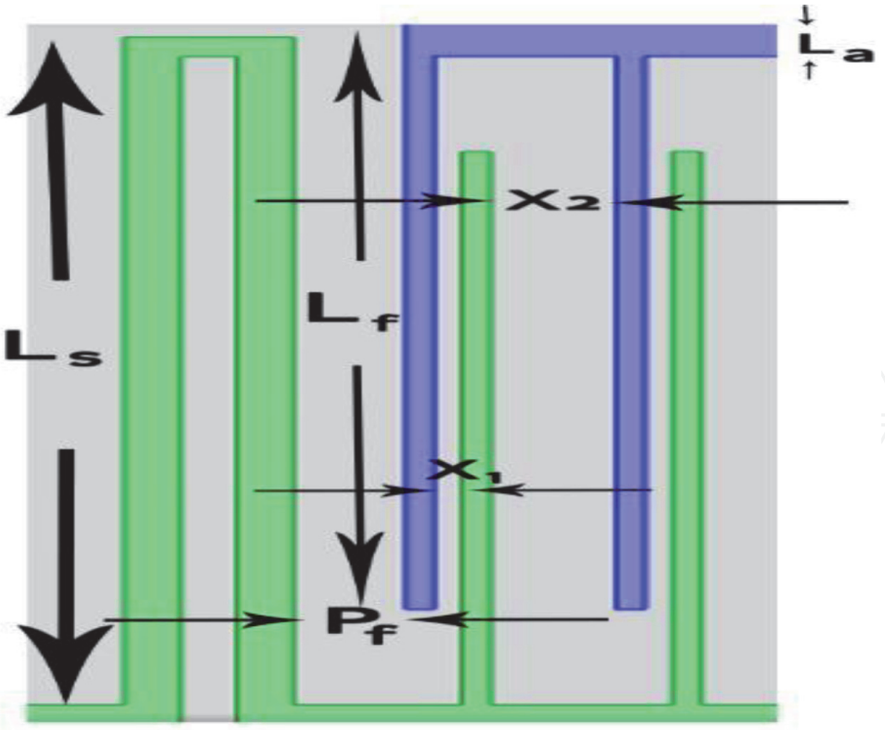

Figure 7.
Different dimensions used in capacitance formulation.

$$C_0 = \left(\frac{K\varepsilon_0 L_{f0} t}{x_1} + \frac{K\varepsilon_0 L_{f0} t}{x_2}\right) \times 2N_f \tag{21}$$

$$C_{pm} = \frac{\varepsilon_0 t W_f (2N_f + 1)}{L_f - L_{f0}} \tag{22}$$

The variation in sensing capacitance value under displacement Δx of the seismic mass is given by.

$$\Delta C = \left(\frac{K\varepsilon_0 L_{f0} t}{x_1}\frac{\Delta x}{x_1} - \frac{K\varepsilon_0 L_{f0} t}{x_2}\frac{\Delta x}{x_2}\right) \times 2N_f \tag{23}$$

Capacitive Sensitivity is given as change in capacitance with respect to applied acceleration $\Delta C/a$ (fF/g).

4. Results and discussions

The device's capacitive sensitivity depends on various geometrical parameters which conflict with each other. Simultaneous optimisation of all design parameters is essential for a highly sensitive device. An optimal problem with the accelerometer-based hearing aid that optimizes both of these variables was formulated mathematically, and simulative analysis was performed using COMSOL. As stated in the authors 'previous work [9], the various geometry parameters have been optimised. The system parameters also need to meet the constraints that need to be taken into account when designing the middle ear implantable microphone. The design constraints are:

- The average sensor length must be within 1 mm.

- The average sensor width must be in 1 mm.
- Sensor resonant frequency shall be 10,000 Hz.
- The sensor must have a total mass of less than 20 mg.

The optimized parameters of the geometry, as shown in **Table 2** [9]. The number of sensing fingers is found to be 174 on each side of the central seismic mass. The spring measurements and the seismic mass are calculated to hold the resonant frequency at about 10,000 Hz. Silicon density is 2330Kg/m3, and its elasticity modulus is 131Gpa. Silicon practically does not exhibit mechanical hysteresis. It therefore constitutes an ideal candidate material for sensors and actuators. Microsystems built and manufactured with silicon provide greater versatility than with other substrate materials. In the proposed research work the entire microsystem consisting of accelerometer and electronics interface circuitry needs to be housed in a biocompatible packaging. Recent advancements show that with minor surface modifications using laser nano texturing could increase the biocompatibility of silicon. Also, silicon compounds like silicon carbide is a promising biocompatible material. The Air is selected as dielectric medium as it offers negligible damping. The aspect ratio which is used is 12.5. Aspect ratio is the structure thickness ratio, and the finger spacing distance. Energy harvesting methodologies may be utilised to provide the power requirements for the proposed device [26–29].

4.1 Sensitivity variation with different spring topologies

Study of the device's output was carried out with different topologies for the spring. Parameters such as the resonant frequency, displacement sensitivity, capacitive sensitivity, seismic mass, and stiffness constants for the same spring beam length of 72 μm are evaluated in **Table 3**. If the number of springs in series rises, the device's displacement and capacitive sensitivity rise as a result of a steady drop in stiffness. The seismic mass and resonant frequency are finding a decrease though. The resonant frequency for our microphone needs to be outside of the usual 8000 Hz hearing range. Although the sensitivity of the device is improved, the combinations of more than one spring can not be approved for the proposed application.

Another alternative is to keep identical resonant frequencies for different combinations as shown in **Table 4**.

Geometry Parameter	Value (μm)
Length of sense finger	100
The width of sense finger	1
Gap spacing (x_1, x_2)	1, 2
The thickness of the device	12.5
Length of spring beam	72
Length of the proof mass	740
The width of the proof mass	884
Width of spring	2

Table 2.
Optimized accelerometer dimensions for the proposed device.

No of springs in combination	Resonant frequency (Hz)	Displacement Sensitivity (nm/g)	Capacitive Sensitivity (fF/g)	Proof mass (ng)	Stiffness constant (Nm/s)
1	10016	2.4771	6.4631	20.079	79.519
2	7606.5	4.2947	11.236	17.406	39.76
3	6750	5.453	14.292	14.734	26.506
4	6461.4	7.1856	15.611	12.061	19.88
5	6550.3	5.7914	15.186	9.3889	15.904

Table 3.
The parameters associated with the different series combination of springs for a similar length.

No of turns in spring	Resonant frequency	Displacement Sensitivity (nm/g)	Capacitive Sensitivity (fF/g)	Proof mass (ng)	Length of spring (μm)	Spring Constant
1	10016	2.4771	6.4631	20.079	72	79.519
2	10019	2.4753	6.4581	17.404	60	68.967
3	10033	2.4688	6.4408	14.731	56	58.536
4	10030	2.4699	6.4437	12.058	54	47.894
5	10021	2.4746	6.456	9.386	55	37.209

Table 4.
The parameters associated with the different series combination of springs for similar resonant frequency.

The orientation of the spring beam	Resonant frequency (Hz)	Displacement (nm/g)	Capacitive Sensitivity (fF/g)	Length of the beam (μm)	Proof mass (ng)	Spring constant (Nm/s)
Folded beam	10016	2.4771	6.4631	72	20.079	79.519
Inverted folded beam	10224	2.377	6.2011	72	20.079	82.867

Table 5.
Comparison of performance of the device with standard folded and inverted folded beam.

It is observed that the displacement and capacitive response are almost identical for different combinations. The length of spring beam needs to be changed to keep the resonant frequencies identical for different combinations. A decline in the seismic mass is noticed with increased number of springs in the arrangement. However, as shown in **Table 4**, no significant change in sensitivity is obtained and the arrangement is of no useful consequence. **Table 5** provides a comparison of regular folded beam sensitivities with inverted folded beam. The regular folded beam provides greater flexibility for the same length of the spring beam (72 μm) than the inverted folded beam.

The output for the spring beam length (72 μm) of folded beam and round folded beam is compared in **Table 6**. The round folded beam has an impressive sensitivity of 8.29 fF/g, an improvement over the regular folded beam. Nonetheless, this substantial improvement comes at the expense of the reduced 8849 Hz resonant frequency (very close to the standard 8000 Hz hearing range). The topology is therefore not suitable for the proposed study.

In **Table 7**, the output of round folded beam was also assessed for similar resonant frequency of 10019 Hz. The strength in this situation is significantly less

Geometry of folded beam	Resonant frequency (Hz)	Displacement Sensitivity (nm/g)	Capacitive Sensitivity (fF/g)	Length of beam (μm)	Proof mass (ng)	Spring constant (Nm/s)
Standard folded beam	10016	2.4771	6.4631	72	20.079	79.519
Round folded beam	8848	3.1736	8.2893	72	20.079	62.066

Table 6.
Comparison of performance of standard folded beam and round folded beam for the same length.

The geometry of the spring beam	Resonant frequency (Hz)	Displacement Sensitivity (nm/g)	Capacitive Sensitivity (fF/g)	Length of the beam (μm)	Proof mass (ng)	Spring constant (Nm/s)
Standard folded beam	10016	2.4771	6.4631	72	20.079	79.519
Round folded beam	10019	2.4756	6.4589	66	20.078	79.564

Table 7.
Comparison of performance of standard folded beam and round folded beam for same resonant frequency.

than the folded beam's. Therefore the option of round folded beam provides no major benefit over the folded beam.

The parameters relating to the configuration of the accelerometer are shown in **Table 8**. The table contrasts the outcomes of the experiment and of simulation. The percentage difference between the analytical and simulation results is less than 10 percent, as is evident from the table. Therefore the findings of the modeling and simulation show strong agreement.

Figure 8 provides the simulation environment for the proposed accelerometer. The First Resonant Frequency is at 10,209 Hz as shown in **Figure 9**. The average stress caused at 100 dB SPL and 10,000 Hz is 0.25 GPa, as shown in **Figure 10**. The average stress is slightly lower than silicon yield power (7 GPa). The yield strength of a material represents the highest stress that can produce without causing plastic deformation in a material. A material exhibits a defined permanent deformation at the stress. Yield strength is very critical in engineering structural design, as it must withstand the force sustained during use when constructing a part, and the part must not permanently deform. Hence the yield strength in any structure must sufficiently exceed the maximum stress produced. The yield strength of silicon (7GPa) in the proposed model is considerably higher than the average stress developed in the structure. COMSOL MULTIPHYSICS simulates the concept with optimized parameters, and validates the effects of the simulations and simulation.

Parameter	Analytical Value	Simulation Value	Error (%)
Resonant Frequency (Hz)	10018	10209	1.87
Nominal Capacitance (pF)	5.17	5.30	2.45
Displacment Sensitivity (nm/g)	2.47	2.65	6.79
Capacitive Sensitivity (fF/g)	6.41	6.89	6.97

Table 8.
Comparison of the analytical and simulation results.

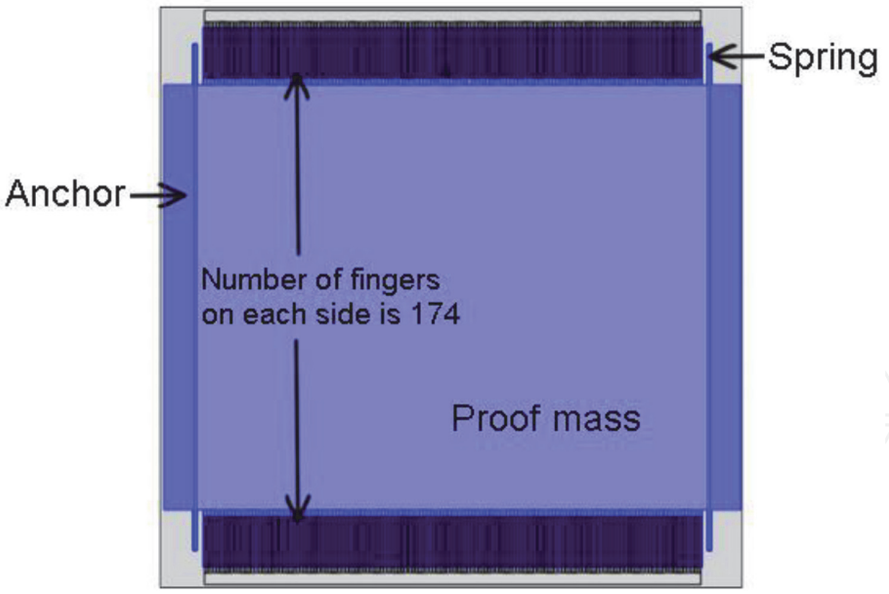

Figure 8.
The simulation setup in COMSOL MULTIPHYSICS.

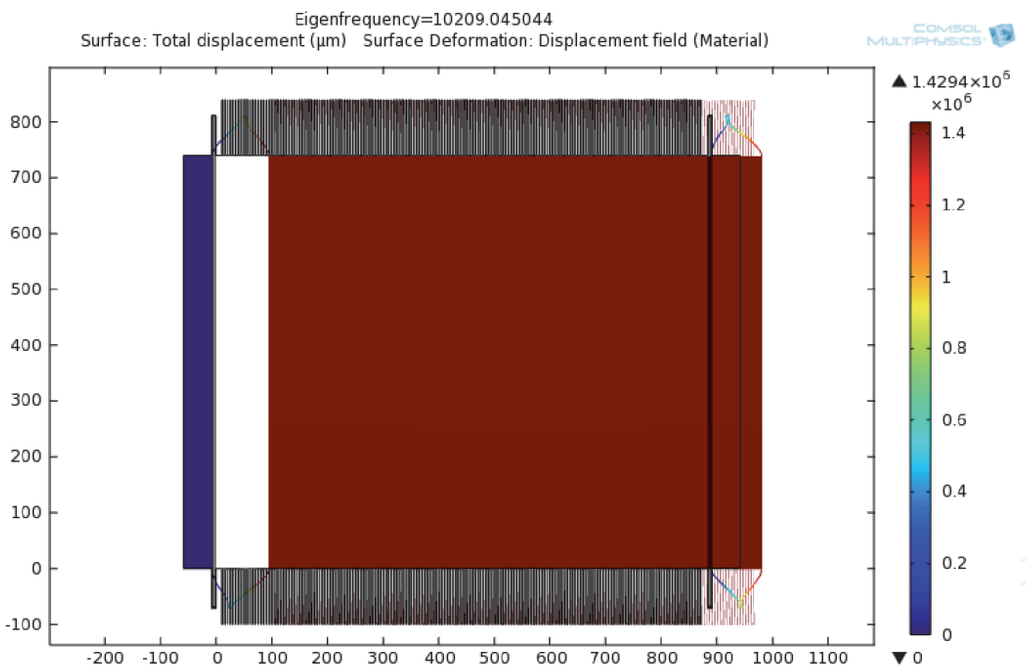

Figure 9.
The first resonant mode of the optimized model.

The proposed accelerometer is compared to previous MEMS capacitive sensors developed by Young et al. [20]. The new design shows an increase in capacitive sensitivity of 27.43 per cent over Young's research as shown in **Table 9**.

Figure 11 shows the proposed accelerometer frequency response conforming to input umbo accelerations of 0.1 g, 0.5 g, and 1.0 g. The device's frequency response is almost flat from 500 Hz to 8000 Hz (the standard conversation range) with a peak at around 10,000 Hz that reflects the accelerometer's first resonant frequency (10,000 Hz). The flat frequency response shall indicate the accelerometer's operating range.

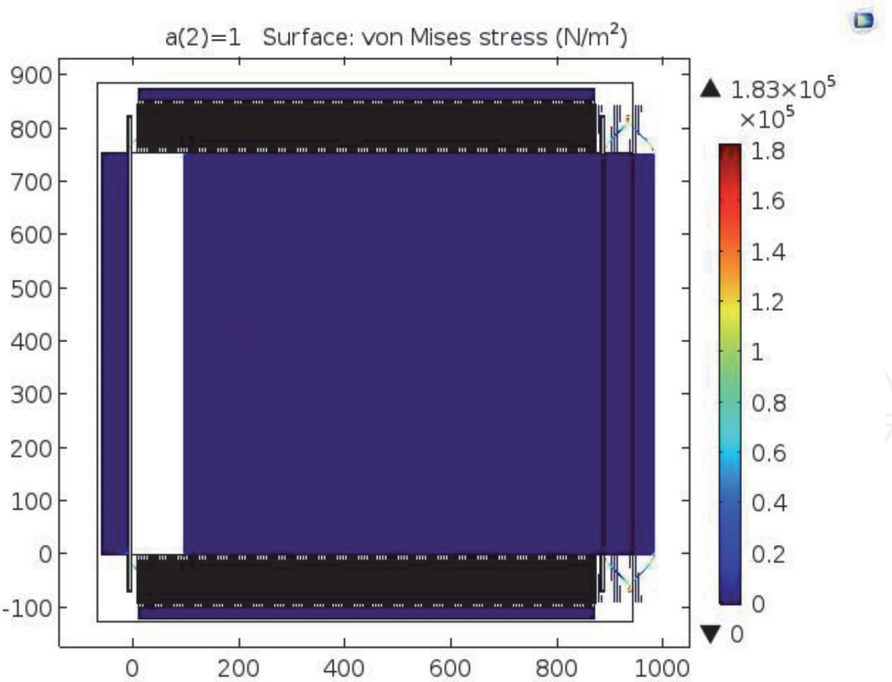

Figure 10.
Maximum stress induced in the optimized model.

Parameter	Proposed Model	Young et al. [20]	Improvement (%)
Resonant Frequency (Hz)	10209	10000	2.04
Nominal Capacitance (pF)	5.30	2.40	54.7
Displacment Sensitivity (nm/g)	2.65	2.50	5.66
Capacitive Sensitivity (fF/g)	6.89	5.00	27.43

Table 9.
Comparison of proposed model with the model of Young et al.

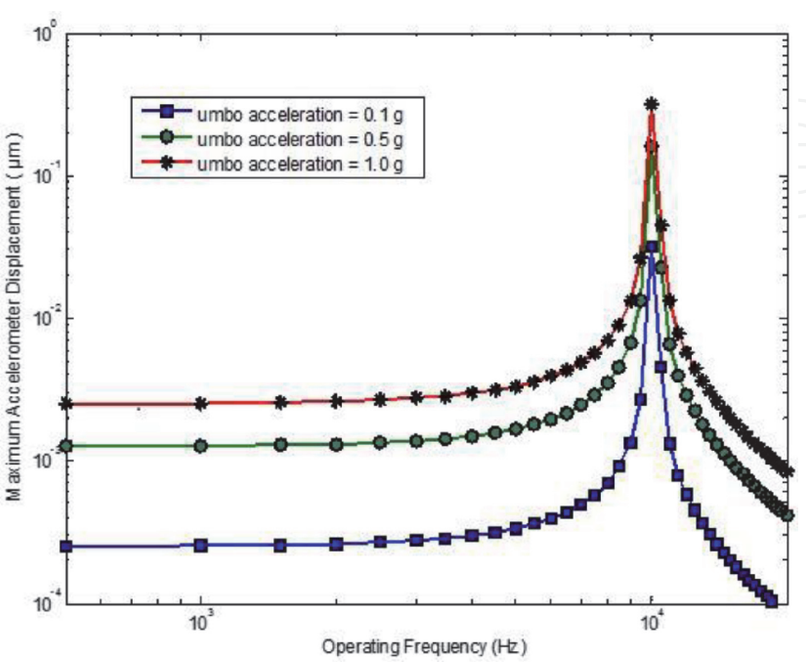

Figure 11.
The frequency response of the optimized model.

5. Conclusion

The research paper proposes an improved MEMS capacitive accelerometer to be used as a microphone for the completely implantable hearing. The effect of different types of suspension systems on accelerometer performance is being studied, and the folded beam spring topology is considered to be the most suitable for the proposed application. The analytical model was developed and validated with simulation results from COMSOL MULTIPHYSICS. The accelerometer occupies a small sensing region of $1mm^2$, an overall packed weight of less than 20 mg and a resonant frequency of almost 10,000 Hz. The accelerometer is designed so it can be inserted surgically and functions well within the standard conversational range of speech. Optimized efficiency of 5.30 pF, displacement sensitivity of 2.65 nm/ g and capacitive sensitivity of 6.89fF/g is achieved with an improvement in sensitivity of 27.43 per cent. The proposed design can therefore be suggested for possible application in totally implantable hearing devices.

Author details

Apoorva Dwivedi[1*], Prateek Asthana[2], Gargi Khanna[1] and Tarun Chaudhary[3]

1 Electronics and Communication Engineering Department, NIT Hamirpur, Hamirpur, Himachal Pradesh, India

2 Bharat Institute of Engineering and Technology, Hyderabad, India

3 Electronics and Communicaion Engineering Department, NIT Jalandhar, Jalandhar, Punjab, India

*Address all correspondence to: apoorva.dwivedi07@gmail.com

References

[1] Wang D. Deep learning reinvents the hearing aid. IEEE spectrum. 2017 Feb 28; 54(3):32-7.

[2] Varshney S. Deafness in India. Indian Journal of Otology. 2016; 22: 73.

[3] Haynes DS, Young JA, Wanna GB, Glasscock III ME. Middle ear implantable hearing devices: an overview. Trends in amplification. 2009 Sep; 13(3):206-14.

[4] Kim MK, Yoon YH, Park IY, Cho JH. Design of differential electromagnetic transducer for implantable middle ear hearing device using finite element method. Sensors and Actuators A: Physical. 2006 Aug 14; 130:234-40.

[5] Häusler R, Stieger C, Bernhard H, Kompis M. A novel implantable hearing system with direct acoustic cochlear stimulation. Audiology and Neurotology. 2008; 13(4):247-56.

[6] Zenner HP, Baumann JW, Reischl G, Plinkert P, Zimmermann R, Mauz PS, Limberger A, Maassen MM. Patient selection for incus body coupling of a totally implantable middle ear implant. Acta oto-laryngologica. 2003 Jun 1; 123 (6):683-96.

[7] Urquiza R, López J, Gonzalez-Herrera A, Povedano V, Ciges M. Tympanic-ossicular prostheses and MEMS technology: whats and whys. Acta oto-laryngologica. 2009 Jan 1; 129 (4):411-5.

[8] Zeng FG, Rebscher S, Harrison W, Sun X, Feng H. Cochlear implants: system design, integration, and evaluation. IEEE reviews in biomedical engineering. 2008 Nov 5; 1:115-42.

[9] Dwivedi A, Khanna G. Sensitivity enhancement of a folded beam MEMS capacitive accelerometer-based microphone for fully implantable hearing application. Biomedical Engineering/Biomedizinische Technik. 2018 Nov 27; 63(6):699-708.

[10] Dwivedi A, Khanna G. Numerical simulation and modelling of a novel MEMS capacitive accelerometer based microphone for fully implantable hearing aid. Microsystem Technologies. 2019 Feb;25(2):399-411.

[11] Dwivedi A, Khanna G. A microelectromechanical system (MEMS) capacitive accelerometer-based microphone with enhanced sensitivity for fully implantable hearing aid: a novel analytical approach. Biomedical Engineering/ Biomedizinische Technik. 2020 Jul 3;1 (ahead-of-print).

[12] Dwivedi A, Asthana P, Khanna G. Effect of Micro Lever Width on the Mechanical Sensitivity of a MEMS Capacitive Accelerometer. InAdvances in VLSI, Communication, and Signal Processing 2020 (pp. 525-532). Springer, Singapore.

[13] Zenner HP, Leysieffer H. Total implantation of the implex TICA hearing amplifier implant for high-frequency sensorineural hearing loss: the tübingen university experience. Otolaryngologic Clinics of North America. 2001 Apr 1; 34(2):417-46.

[14] Briggs RJ, Eder HC, Seligman PM, Cowan RS, Plant KL, Dalton J, Money DK, Patrick JF. Initial clinical experience with a totally implantable cochlear implant research device. Otology & Neurotology. 2008 Feb 1; 29 (2):114-9.

[15] Bruschini LU, Forli FR, Santoro A, Bruschini PA, Berrettini ST. Fully implantable Otologics MET Carina™ device for the treatment of sensorineural hearing loss. Preliminary surgical and clinical results. Acta

Otorhinolaryngologica Italica. 2009 Apr; 29(2):79.

[16] Pulcherio JO, Bittencourt AG, Burke PR, da Costa Monsanto R, De Brito R, Tsuji RK, Bento RF. Carina® and Esteem®: a systematic review of fully implantable hearing devices. PLoS One. 2014 Oct 17; 9(10):e110636.

[17] Kraus EM, Shohet JA, Catalano PJ. Envoy esteem totally implantable hearing system: phase 2 trial, 1-year hearing results. Otolaryngology–Head and Neck Surgery. 2011 Jul; 145(1): 100-9.

[18] Ko WH, Zhang R, Huang P, Guo J, Ye X, Young DJ, Megerian CA. Studies of MEMS acoustic sensors as implantable microphones for totally implantable hearing-aid systems. IEEE Transactions on Biomedical Circuits and Systems. 2009 Sep 25; 3(5):277-85.

[19] Zurcher MA, Semaan M, Megerian CA, Ko WH, Young DJ. A MEMS capacitive accelerometer design as middle ear microphone based on ossicular chain micromechanic characterization at umbo for fully implantable cochlear prosthesis. Sensors and Materials. 2010 Jan 1; 22(6):297-312.

[20] Young DJ, Zurcher MA, Semaan M, Megerian CA, Ko WH. MEMS capacitive accelerometer-based middle ear microphone. IEEE Transactions on Biomedical Engineering. 2012 Apr 20; 59(12):3283-92.

[21] Yip M, Jin R, Nakajima HH, Stankovic KM, Chandrakasan AP. A fully-implantable cochlear implant SoC with piezoelectric middle-ear sensor and arbitrary waveform neural stimulation. IEEE journal of solid-state circuits. 2014 Sep 25; 50(1):214-29.

[22] Woo ST, Shin DH, Lim HG, Seong KW, Gottlieb P, Puria S, Lee KY, Cho JH. A new trans-tympanic microphone approach for fully implantable hearing devices. Sensors. 2015 Sep; 15(9):22798-810.

[23] Koch M, Eßinger TM, Stoppe T, Lasurashvili N, Bornitz M, Zahnert T. Fully implantable hearing aid in the incudostapedial joint gap. Hearing research. 2016 Oct 1; 340:169-78.

[24] Wai-Chi W, Azid AA, Majlis BY. Formulation of stiffness constant and effective mass for a folded beam. Archives of Mechanics. 2010 Apr 11; 62 (5):405-18.

[25] Wong WC, Azid IA, Majlis BY. Theoretical analysis of stiffness constant and effective mass for a round-folded beam in MEMS accelerometer. Strojniški vestnik-Journal of Mechanical Engineering. 2011 Jun 15; 57(6):517-25.

[26] Asthana P, Khanna G. Finite-element modeling of piezoelectric energy harvesters using lead-based and lead-free materials for voltage generation. Journal of Asian Ceramic Societies. 2018 Oct 2; 6(4):394-400.

[27] Asthana P, Khanna G. A broadband piezoelectric energy harvester for IoT based applications. Microelectronics Journal. 2019 Nov 1; 93:104635.

[28] Asthana P, Dwivedi A, Khanna G. Finite Element Modeling of a Wideband Piezoelectric Energy Harvester for Ambient Vibration Extraction. InAdvances in VLSI, Communication, and Signal Processing 2020 (pp. 549-556). Springer, Singapore.

[29] Asthana P, Khanna G. Power amplification interface circuit for broadband piezoelectric energy harvester. Microelectronics Journal. 2020 Apr 1; 98:104734.